Materials Science & Engineering C 92 (2018) 849–861

Contents lists available at ScienceDirect

Materials Science & Engineering C

journal homepage: www.elsevier.com/locate/msec

Characterization of chemically treated Ti-Zr system alloys for dental implant application

Jairo M. Cordeiro[a,b,1], Leonardo P. Faverani[c,1], Carlos R. Grandini[b,d], Elidiane C. Rangel[e], Nilson C. da Cruz[e], Francisco H. Nociti Junior[a], Amanda B. Almeida[a], Fabio B. Vicente[b,f], Bruna R.G. Morais[c], Valentim A.R. Barão[a,b,*,2], Wirley G. Assunção[g,2]

[a] University of Campinas (UNICAMP), Piracicaba Dental School, Department of Prosthodontics and Periodontology, Av Limeira, 901, Piracicaba, São Paulo 13414-903, Brazil
[b] Institute of Biomaterials, Tribocorrosion and Nanomedicine (IBTN), Brazil
[c] Univ Estadual Paulista (UNESP), Aracatuba Dental School, Department of Surgery and Integrated Clinic, R. José Bonifácio, 1193, Aracatuba, São Paulo 16015-050, Brazil
[d] Univ Estadual Paulista (UNESP), Laboratório de Anelasticidade e Biomateriais, Av. Eng. Luiz Edmundo Carrijo Coube, Bauru, São Paulo 17033-360, Brazil
[e] Univ Estadual Paulista (UNESP), ICTS, Laboratory of Technological Plasmas, Av Três de Março, 511, Sorocaba, São Paulo 18087-180, Brazil
[f] Universidade Paulista (UNIP), Av. Luís Levorato, 1-40, Bauru, São Paulo 17048-290, Brazil
[g] Univ Estadual Paulista (UNESP), Aracatuba Dental School, Department of Dental Materials and Prosthodontics, R. José Bonifácio, 1193, Aracatuba, São Paulo 16015-050, Brazil

ARTICLE INFO

Keywords:
Alloys
Titanium
Zirconium
Dental implant
Corrosion

ABSTRACT

Materials and surfaces developed for dental implants need to withstand degradation processes that take place in the oral cavity. Therefore, the aim of the study was to develop and evaluate the topographical, mechanical, chemical, electrochemical and biological properties of Ti-xZr alloys (x = 5, 10, and 15 wt%) with two surface features (machined and double acid etched). Commercially pure titanium (cpTi) and Ti-6Al-4V alloy were used as controls. Surface characterization was performed using dispersive energy spectroscopy, X-ray diffraction, scanning electron microscopy, atomic force microscopy, profilometry and surface energy. The mechanical properties were assessed using Vickers microhardness, elastic modulus and stiffness. The electrochemical behavior analysis was conducted in a body fluid solution (pH 7.4). In addition, MC3T3-E1 cells were used to determine the impact of material and surface treatment on cell morphology by SEM analysis. Data were analyzed by two-way ANOVA and Bonferroni test ($\alpha = 0.05$). Ti-Zr alloys showed lower surface roughness, elastic modulus and stiffness, as well as higher hardness and surface energy when compared to cpTi. Ti-Zr system increased the polarization resistance values and significantly decreased the capacitance, corrosion current density (i_{corr}), and passivation current density (i_{pass}) values. The acid treatment increased the resistance and corrosion potential of the oxide layer. SEM data analysis demonstrated that Ti-Zr alloys displayed normal cell attachment/spreading and slightly changed cell morphology in the double etched surface. In conclusion, Zr addition and surface treatment altered surface, mechanical, biological and electrochemical properties of Ti material.

1. Introduction

Titanium (Ti) alloys have emerged in dentistry as viable options for rehabilitation with dental implants [1], especially in situations where the use of commercially pure titanium (cpTi) is not feasible. Applications involving extensive defect treatments, areas under high loads, or cases that require implants with reduced dimensions [2,3] are conditions that demand materials with superior properties, generally achieved by adding chemical elements to Ti. Besides that, implants are exposed to complications of a mechanical or biological nature [4], such as fracture [5], the stress shielding effect [6], overloading, osseointegration failure, peri-implantitis [7], and corrosion and wear

* Corresponding author at: Av. Limeira, 901, Piracicaba, SP 13414-903, Brazil.
E-mail address: vbarao@unicamp.br (V.A.R. Barão).
[1] These authors contribute equally to this work.
[2] These authors jointly supervised this work.

https://doi.org/10.1016/j.msec.2018.07.046
Received 3 October 2017; Received in revised form 11 June 2018; Accepted 18 July 2018
Available online 19 July 2018
0928-4931/

degradation processes that can lead to inflammation and allergenic or toxic reactions [8].

For a long period, Ti-6Al-4V alloy was the first choice for clinically challenging situations, mainly because of its enhanced mechanical performance. However, this material has been considered to have a highly stimulatory nature due to the release of ions and debris, which may play a critical role in stimulating peri-implant inflammation and osteolysis [9] due to its toxic potential [10]. Thus, an ideal material must offer high levels of mechanical stability without releasing metal ions into the human body. In this context, the binary Ti-Zr alloy has gained much attention, since this system guarantees increased mechanical strength with extensive applications [2,11], showing a remarkable decrease in ion release [12], which demonstrates its more inert and biocompatible behavior in comparison with cpTi [13,14]. Additionally, its homogeneous α-phase microstructure ensures that surface modification processes used for enhancing the osseointegration of Ti can still be applied to Ti-Zr implants [2,15].

This fact is of great concern, since the optimization of implant surface chemistry and topography has been crucial to promote cell adhesion, differentiation, and proliferation, as well as to increase the corrosion resistance [16]. Among the surface treatments developed in recent years, the process involving sandblasting followed by acid etching (SLA) of the implants is one of the most successfully applied in clinics [17]. Treatments that produce surfaces similar to those obtained by SLA but without the grit blasting process have been proposed. These surfaces are achieved by means of double acid etching, which appears to have the potential to greatly enhance osseointegration without adding particulate matter or embedding surface contaminants [18]. The biological [18,19] and corrosion behaviors [20] of this type of surface have been evaluated when applied in cpTi and Ti-Al-V alloys. However, the effect of such etching treatment on promising Ti-Zr alloys with different Zr concentrations has not yet been studied.

Therefore, this study developed and accessed the surface, mechanical, electrochemical, and biological properties of binary Ti-xZr (x = 5, 10, and 15 wt%) alloys considering two surface features: machined and double acid etched. CpTi and Ti–6Al–4 V alloys, which are widely used for the manufacture of dental implants, were used as controls.

2. Materials and methods

2.1. Experimental design

Fig. 1 shows the experimental design of this study. The machined surface was obtained by a polishing process, while the double etched group was chemically treated with acids (nitric, sulfuric, and hydrochloric acid) according to standard procedures (Military Institute of Engineering – IME, Rio de Janeiro, Brazil). CpTi and Ti–6Al–4V alloys were obtained in the shape of discs, 10 mm in diameter and 2 mm thick (Implalife Biotecnologia, Jales, SP, Brazil). Ti-x%Zr (x = 5, 10, and 15) alloys were fabricated from pure metals.

2.2. Fabrication of experimental alloys

The three experimental binary Ti-Zr alloys (Ti-5Zr, Ti-10Zr, and Ti-15Zr) (wt%) were melted from pure metals (Ti and Zr presented degrees of purity equal or superior to 99.0%) (Sigma-Aldrich, St. Louis, MO, USA) in an arc-voltaic furnace with a water-cooled copper crucible under an argon atmosphere. The ingots were remelted five times to ensure homogeneity of the samples [11,21]. All ingots were heated to 1000 °C and hot-swaged to form bars ≈ 11 mm in diameter. Then, ingots were fitted in quartz tubes, heat-treated at 1000 °C for 1 h, and air-cooled to improve the alloys' mechanical behavior [21]. Ti-Zr bars were machined into discs (10 mm in diameter and 2 mm thick).

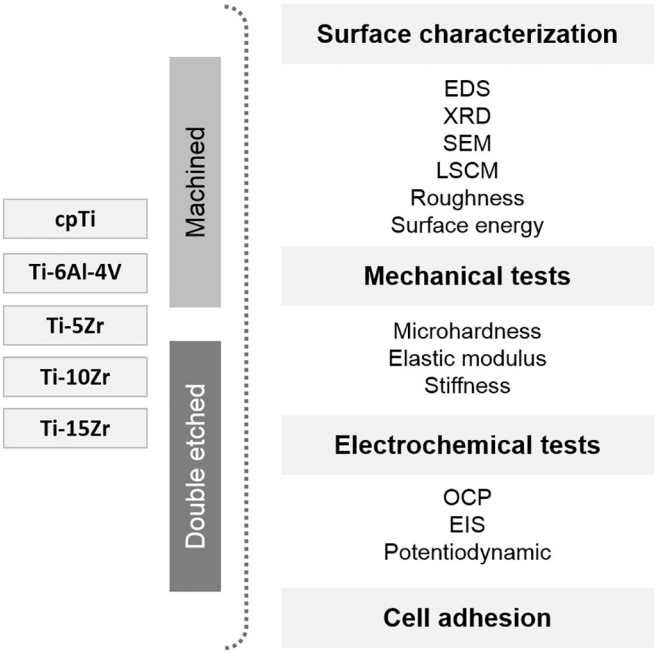

Fig. 1. Schematic diagram of the experimental design. EDS = energy-dispersive spectroscopy; XRD = X-ray diffractometry; SEM = scanning electron microscopy; LSCM = laser scanning confocal microscopy; OCP = open circuit potential; and EIS = electrochemical impedance spectroscopy.

2.3. Surface preparation

All discs were polished with #320-, #400-, and #600-grit SiC abrasive papers (Carbimet 2, Buehler, Lake Bluff, IL, USA) in an automatic polisher (EcoMet 300 Pro with AutoMet 250; Buehler, Lake Bluff, IL, USA). The surfaces that resulted from this process were considered as the machined surfaces.

The double etched surfaces were obtained according to proprietary standards (IME, Rio de Janeiro, Brazil). After being polished, the discs were chemically treated with a double acid etching (sulfuric and hydrochloric acid) process for 1 h and 50 min [20]. After surface preparation, all samples were ultrasonically cleaned/degreased with deionized water (10 min) and 70% propanol (10 min) (Sigma-Aldrich, St. Louis, MO, USA) and dried with warm air.

2.4. Surface characterizations

The samples' chemical compositions (in the order of 1 μm^3) were checked by energy-dispersive spectroscopy (EDS) (n = 1). The microstructural analysis of the cpTi and Ti alloys were determined by X-ray diffractometry (XRD; Panalytical, X_Pert3 Powder, Almelo, The Netherlands) using Cu–Kα (λ = 1.540598 Å) radiation and operating at 45 kV and 40 mA at a continuous speed of 0.02° per second and a scan range from 20° to 80° (n = 1). Scanning electron microscopy (SEM; JEOL JSM-6010LA, Peabody, MA, USA) was used to confirm the material microstructural phases after a specific polishing protocol that is followed by the surface etching with Kroll's reagent (5% nitric acid, 10% hydrofluoric acid, and 85% water) (Sigma–Aldrich, St. Louis, MO, USA) [21]. SEM and 3D Laser Scanning Confocal Microscope (LSCM, VK-X200 series, Keyence, Osaka, Japan) were used to observe the surface morphology and topography (n = 1). The LSCM images were obtained with lenses of 50× and 150× magnifications. VK-Analyzer software (Keyence v3.3.0.0) was used for image processing and surface area acquirement, which was achieved by the extrapolation of its measurements in images of 100 × 100 μm (50× magnification) [22]. The average roughness (Ra) (n = 5) and surface free energy (n = 5) were evaluated by a profilometer (Dektak 150-d; Veeco, Plainview, NY,

USA) and an automated goniometer (Ramé-Hart 100–00; Ramé-Hart Instrument Co., Succasunna, NJ, USA), respectively [21].

2.5. Mechanical tests

The Vickers hardness (n = 5) was measured by means of an indenter (Shimadzu, HMV-2 Micro Hardness Tester, Shimadzu Corporation, Kyoto, Japan). The applied load was 0.5 kgf for 15 s. The test was performed at four randomly distributed points in each sample. The values of Vickers hardness were calculated according to the following formula: $Hv = 1.8544P / d^2$, where P = applied load and d = length of the diagonals of indentations [20]. A nano-indenter (TI 950 TriboIndente, Hysitron Inc., Eden Prairie, MN, USA) equipped with a diamond Berkovich-type indenter (100 nm in diameter) was used to measure the elastic modulus and stiffness. Indentations were performed in at least five positions of each sample, with a trapezoidal load function with 2 mN of maximum force. The loading, unloading, and dwell times were 5, 5, and 2 s, respectively.

2.6. Corrosion assessment

A standardized method of three-electrode cells, as required by ASTM International (formerly the American Society for Testing and Materials – ASTM) (G61–86 and G31–72), associated with a potentiostat (Interface 1000, Gamry Instruments, Warminster, PA, USA) was used to assess the samples' electrochemical behavior. The exposed surface of the sample was kept in contact with simulated body fluid (SBF) at 37 ± 1 °C (pH 7.4), which was used to mimic the blood plasma. In total, a 10-mL quantity of electrolyte was used for each corrosion experiment [23]. The chemical composition of the SBF (in grams per liter) was NaCl (12.0045), $NaHCO_3$ (0.5025), KCl (0.3360), K_2HPO_4 (0.2610), Na_2SO_4 (0.1065), 1 M HCl (60 mL), $CaCl_2{\cdot}2H_2O$ (0.5520), and $MgCl_2{\cdot}H_2O$ (0.4575) [24]. Tris was used to achieve a pH of 7.4. The estimated exposed area (in square centimeters) of materials was determined by LSCM and can be seen in Table 1.

The corrosion assessment was carried out according to a specific protocol [20,23]. Firstly, the sample oxide layer was standardized by applying a cathodic potential (−0.9 V vs. SCE - Saturate Calomel Electrode) for 10 min. Then, the free corrosion potential of the material in the electrolyte solution was measured by the open circuit potential (OCP) (3600 s). Afterwards, electrochemical impedance spectroscopy (EIS) was performed at frequencies of 100 kHz to 5 mHz, with an AC curve in the range of ± 10 mV applied to the electrode at its corrosion potential. The real (Z′) and imaginary (Z″) components of impedance were determined and used to construct Nyquist, Bode (|Z|), and phase angle plots. Echem Analyst software (Gamry Instruments, Warminster, PA, USA) was used to analyze the EIS data. An equivalent electrical circuit was fitted for quantification of the corrosion process in the passive/oxide film formation (polarization resistance, R_p, and constant phase element, CPE).

Finally, the samples were polarized from −0.8 to 1.8 V (scan rate of 2 mV/s). Corrosion parameters such as E_{corr} (corrosion potential), i_{corr} (corrosion current density), and Tafel slopes (bc, ba) were obtained from the potentiodynamic polarization curves by the Tafel extrapolation method (Echem Analyst Software, Gamry Instruments, Warminster, PA, USA). The passivation current density (i_{pass}) corresponds to the current value of the passivation region of the polarization plot. The electrochemical tests were conducted at least five times (n = 5) to ensure reliability and reproducibility.

Table 1
Estimated exposed area (cm^2) obtained by LSCM of machined and double etched cpTi and Ti alloy surfaces (n = 1).

	Material	Area (cm^2)
Machined	cpTi	0.90
	Ti-6Al-4V	0.82
	Ti-5Zr	0.86
	Ti-10Zr	0.83
	Ti-15Zr	0.83
Double etched	cpTi	2.39
	Ti-6Al-4V	1.50
	Ti-5Zr	1.98
	Ti-10Zr	1.25
	Ti-15Zr	1.32

2.7. Cell culture

A pre-osteoblastic cell line (MC3T3-E1) was expanded in Minimum Essential Medium Eagle – Alpha Modification (Alpha MEM: Gibco, Life Technologies, Gaithersburg, MD, USA) supplemented with 10% fetal bovine serum (FBS; Gibco, Life Technologies, Gaithersburg, MD, USA), penicillin (100 U/mL), and streptomycin (100 mg/mL) in a humidified incubator at 37 °C and 5% CO_2 atmosphere. After cell expansion, low passage cells were counted and seeded on autoclaved discs in triplicate at 1.5×10^4 cells/mL in a 24-well plate for 96 h in culture medium (Alpha MEM) supplemented with 2% FBS plus antibiotics. Cell morphology and adhesion were determined by SEM (JEOL JSM-5600LV, Peabody, MA, USA). Sample preparation followed a previously reported protocol [25].

2.8. Statistical analyses

The normality of all response variables was tested by the Shapiro–Wilk method. Two-way ANOVA was used to test the statistically significant differences among materials (factor 1, five levels) as a function of the surface type (factor 2, two levels). The Bonferroni test was used as a post hoc technique for multiple comparisons. A mean difference significant at the 0.05 level was used for all tests (SPSS v. 20.0, SPSS Inc.).

3. Results

3.1. Surface and microstructure characterizations

The distribution maps of the elements that constitute the samples and their concentrations (wt%) obtained by means of semi-quantitative EDS analysis are shown in Fig. 2. It can be observed that alloying elements were well distributed, and no relevant contamination was detected. In all cases, the concentrations of the alloying elements (V and Zr) were increased in the double etched surface.

The XRD patterns (Fig. 3) of machined and double etched surfaces showed that the addition of Zr to Ti has not changed its microstructure, which remains as a hexagonal α phase. On the other hand, Ti-6Al-4V alloy exhibit a two-phase (α + β) structure. These features can be confirmed by the SEM images (2000×) (Fig. 4). After being etched with Kroll's reagent, the grain boundary of the equiaxed α structure for cpTi and Ti-5Zr can be observed. The Ti-10Zr and Ti-15Zr exhibited the Widmanstätten pattern, which is characterized by a lamellar and fine needle-like structure. For Ti-Al-V, β phase dispersed in an α matrix can be noticed. Regarding to the double etched surfaces, Ti-Al-V alloy presented the intermetallic compound $Al_5Ti_3V_2$ while Ti-5Zr and Ti-10Zr showed residual Zr in the XRD assessment. Besides, Ti hydride (TiH) was found in the cpTi and Ti-Zr alloys etched surfaces.

The surface morphologies of the cpTi and Ti alloys observed by SEM and LSCM are shown in Figs. 4 and 5. The polishing process resulted in longitudinal grooves in the machined surfaces of all materials. The double acid etching process created an irregular and complex microtopography. The SEM micrographs reveal a porous surface (hole diameter < 10 μm) with pits. Especially for Ti-Al-V, it is possible to observe pores and pits of much smaller dimensions than are found in the other groups. On the other hand, a distinct surface of the Ti-Zr alloys is clearly visible. In these alloys, the pits followed the microstructural

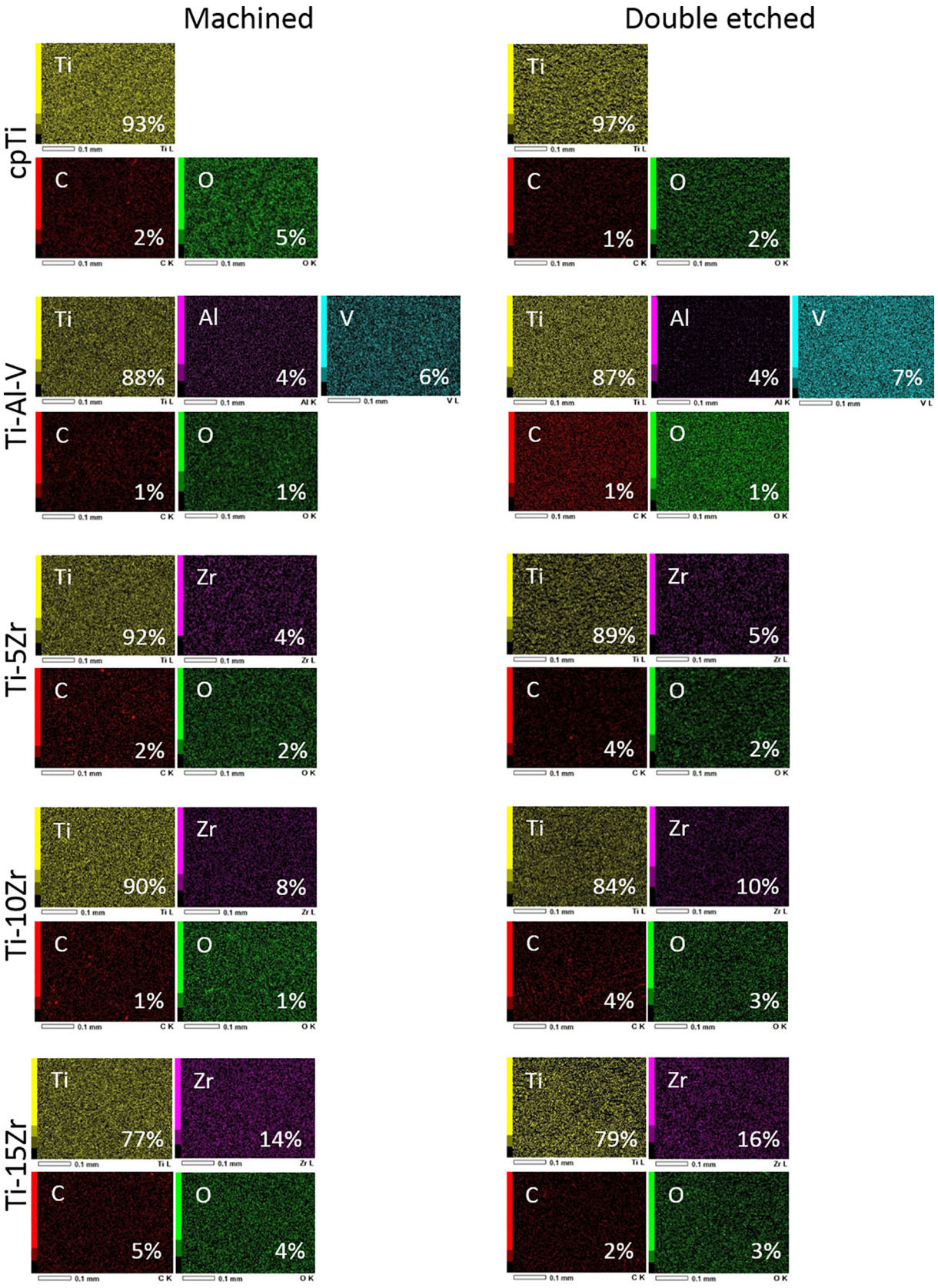

Fig. 2. Chemical mapping by EDS with element concentrations (wt%) for machined and double etched cpTi and Ti alloys surfaces.

characteristics of the material, such as the grain orientation, size, and shape. Concerning to the three-dimensional images obtained by LSCM, the Ti-5Zr alloy presented the most distinct machined surface, which showed less grooves and more surface projections. With regard to the double etched surfaces, Ti-Al-V and Ti-15Zr alloys presented more uniform and homogenous surfaces, while cpTi, Ti-5Zr and Ti-10Zr

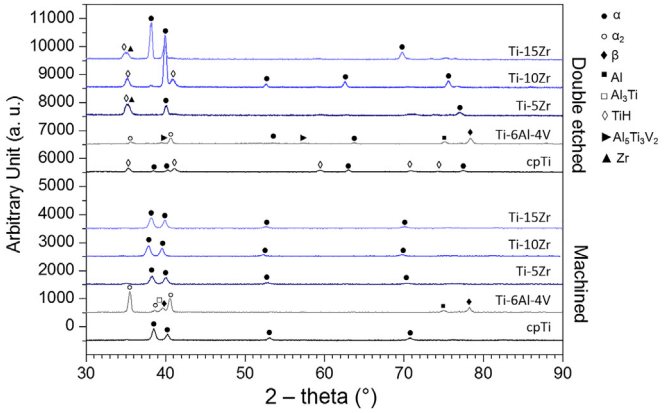

Fig. 3. X-ray diffraction patterns of machined and double etched cpTi and Ti alloy surfaces.

alloys showed evident valleys and peaks. These differences are mainly due to the microstructural features of each material.

Fig. 6a shows the average roughness of all surfaces. For machined group, cpTi presented the highest roughness ($p < 0.05$), while the other materials had similar roughness. Topographic changes caused by the acid etching resulted in a significant increase in the average roughness of all materials ($p < 0.05$), where the Ti-15Zr etched surface presented the highest values ($p < 0.05$). Regarding to the surface energy (Fig. 6b), the addition of Zr in the Ti material promoted greater surface energy for the machined condition ($p < 0.05$). Interestingly, the acid etching process only increased the surface energy of cpTi and Ti-Al-V ($p < 0.05$). However, all treated samples tend to present similar values. Despite the differences, all materials showed predominantly hydrophilic behavior, having water contact angles lower than 90° (data not shown).

3.2. Mechanical properties

Concerning to hardness property (Fig. 7), Ti-Zr alloys stand out due to their higher hardness ($p < 0.05$) than control groups. A statistically significant increase in hardness was observed for double etched surfaces versus machined surfaces ($p < 0.05$), with the exception of Ti-10Zr alloy. Table 2 presents the elastic modulus and stiffness of the cpTi and Ti alloys. Both properties were assessed only for machined surfaces, since the technique used cannot be practicable on the irregular double etched topography. As can be observed, cpTi has the lowest elastic modulus ($p < 0.05$) followed by Ti-5Zr and Ti-15Zr. These three materials also have lower values of stiffness ($p < 0.05$) compared to Ti-Al-V and Ti-10Zr.

3.3. Electrochemical assessment

Fig. 8 shows the evolution in the OCP of machined and double

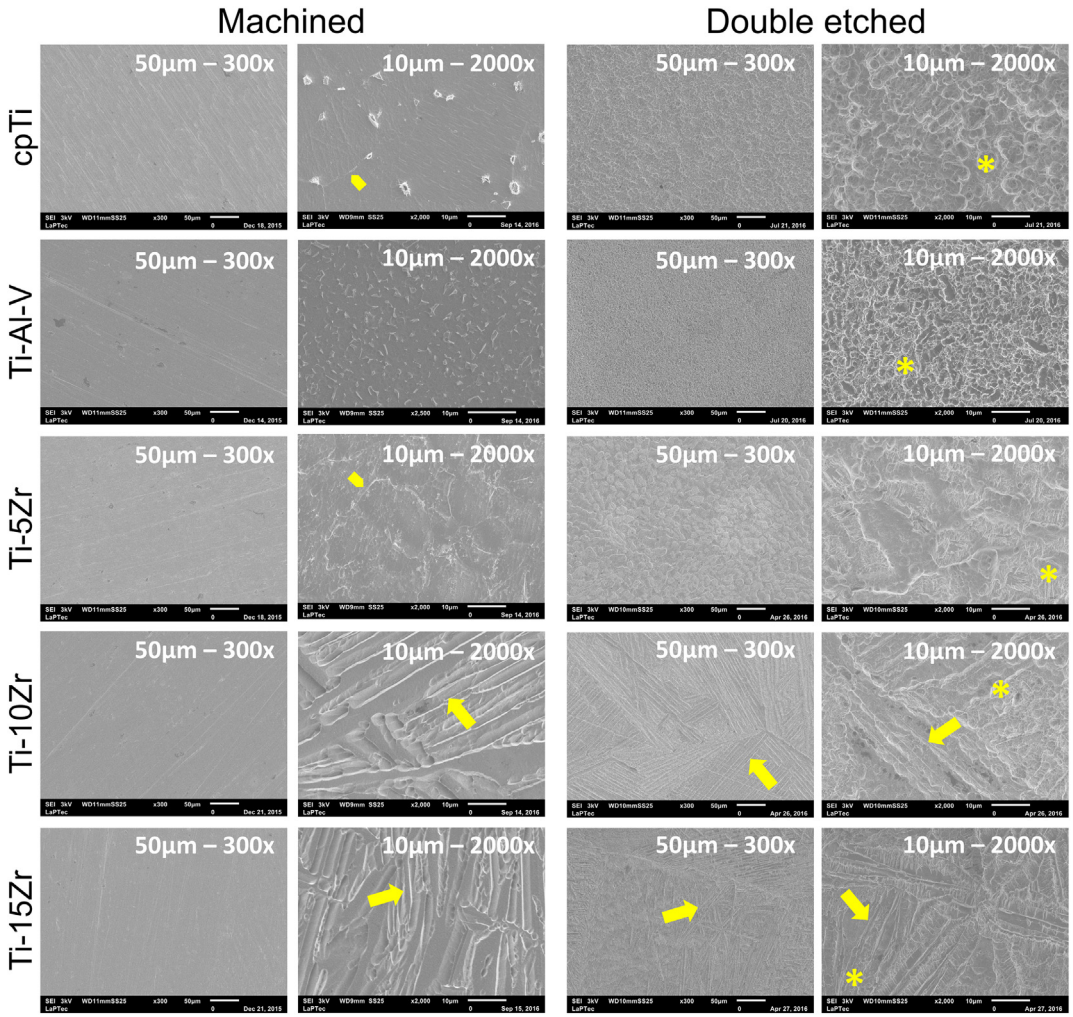

Fig. 4. SEM micrographs of machined and double etched cpTi and Ti alloys surfaces. Images of 2000× from machined group were obtained after treatment with Kroll's reagent. Pentagons shows the grain boundaries. Asterisks indicate the holes and pits on the surface. Arrows indicate the lamellae and fine needle-like structure.

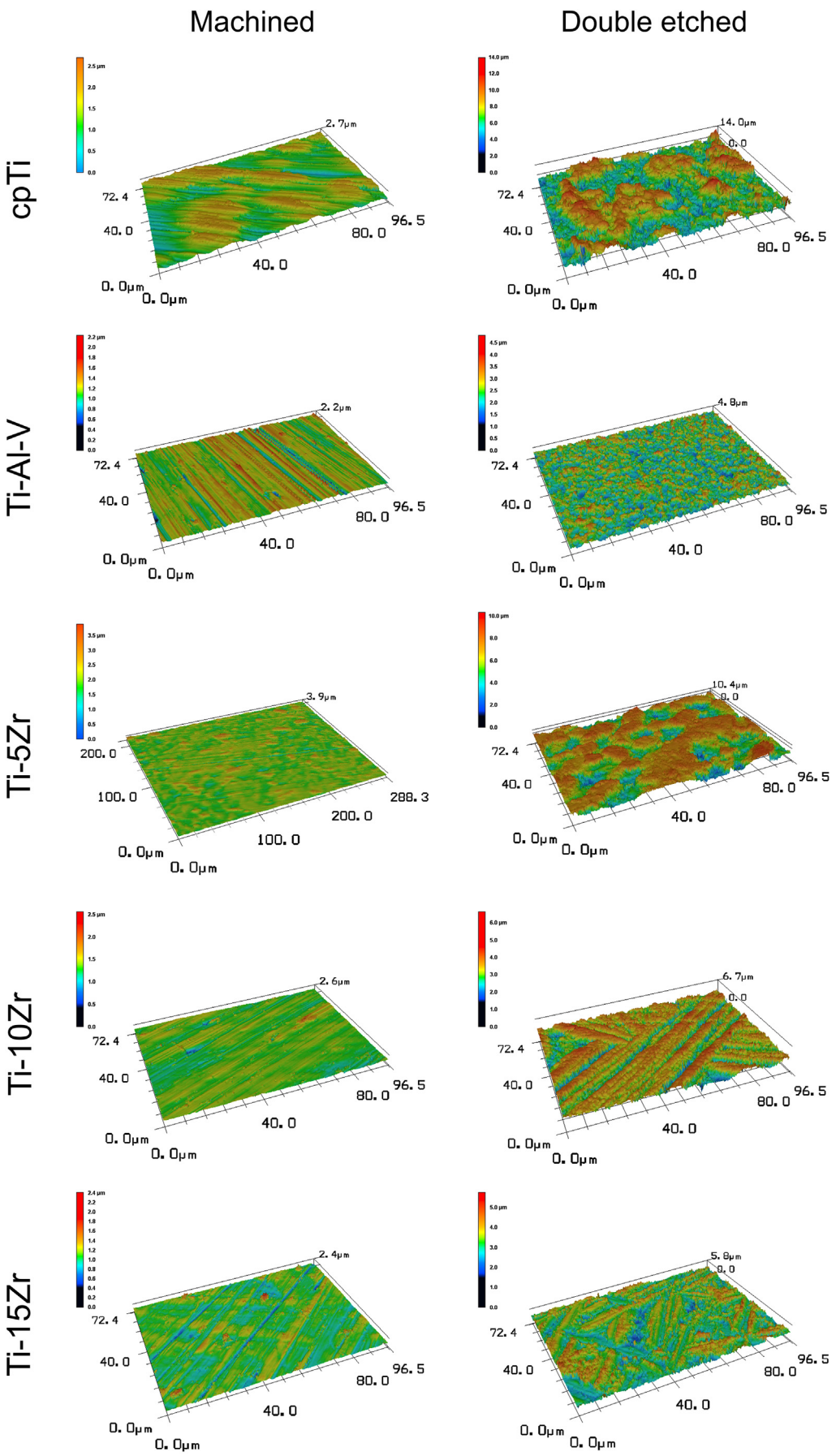

Fig. 5. Three-dimensional LCSM images of machined and double etched cpTi and Ti alloy surfaces.

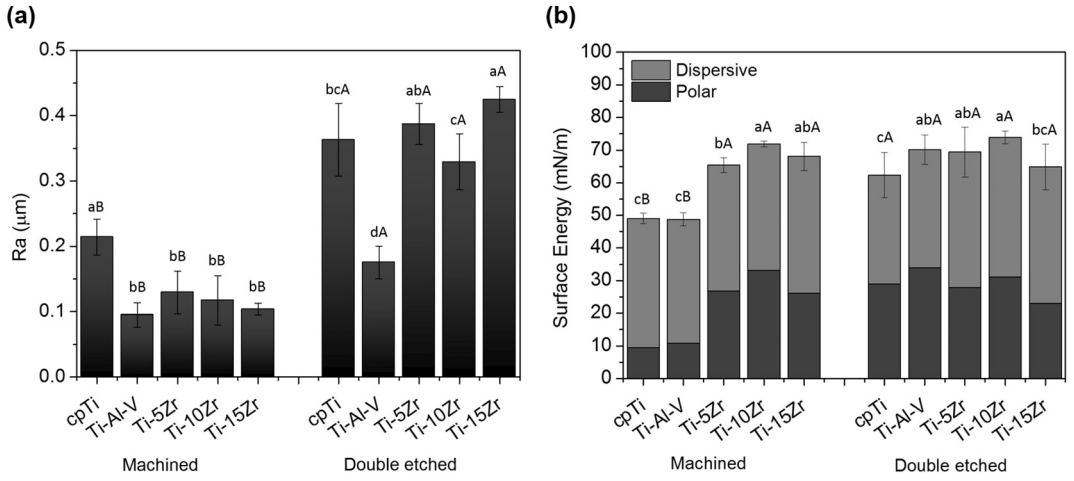

Fig. 6. Average roughness (Ra) (n = 5) (a) and surface energy (n = 5) (b) of machined and double etched cpTi and Ti alloy surfaces. Different lowercase letters indicate statistically significant differences among the materials within each surface type. Different capital letters indicate statistically significant differences between the surfaces of each material ($p < 0.05$, Bonferroni test).

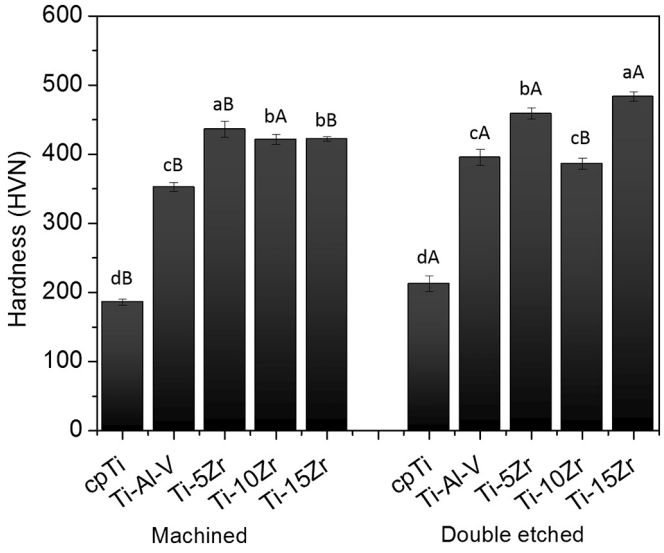

Fig. 7. Surface hardness (n = 5) of machined and double etched cpTi and Ti alloy surfaces. Different lowercase letters indicate statistically significant differences among the materials within each surface type. Different capital letters indicate statistically significant differences between the surfaces of each material ($p < 0.05$, Bonferroni test).

Table 2
Mean (and standard deviation) of elastic modulus and stiffness of machined cpTi and Ti alloy (n = 1).

Material	Elastic modulus (GPa)	Stiffness (μN/nm)
cpTi	104.58 (4.03)d	82.51 (2.82)b
Ti-6Al-4V	143.60 (5.21)a	97.89 (5.81)a
Ti-5Zr	115.42 (8.47)c	77.97 (2.49)b
Ti-10Zr	134.90 (2.75)a	96.99 (1.59)a
Ti-15Zr	125.33 (5.73)b	81.79 (2.14)b

Means followed by different lowercase letters indicate statistically significant differences among the materials.

etched surfaces for 1 h. It can be seen that the free potential of all materials remained stable after a few minutes. The values after 1 h are summarized in Table 3. Ti-5Zr presented the noblest behavior among untreated materials as its potential shifted to more electropositive values ($p < 0.05$). The acid etching statistically enhanced the electrochemical potential of all materials, which may indicate a lower tendency to lose electrons to the environment.

The corrosion properties of the materials and surfaces were evaluated by EIS. On analyzing the Nyquist (Fig. 9) and Bode plots (Fig. 10) of machined surfaces, the superior capacitive behavior of the alloys is remarkable. Ti-Zr alloys exhibited open arches with large diameters. In addition, Ti-Zr alloys presented higher phase angles ($-\Theta$) and greater impedance ($|Z|$) values than cpTi and Ti-Al-V, indicating a more protective oxide layer. The double etched surfaces showed increased arches diameters in the Nyquist plot, as well as slightly increase in the impedance and phase angles values.

Only one time constant was observed for all materials in the phase angle, suggesting the formation of a single compact film on the surface. For this reason, EIS data were fitted using a simple electrical circuit consisting of R_{sol} (resistance of the electrolyte), R_p (polarization resistance), and Q (constant phase element) to obtain the corrosion parameters (Table 4). The good quality of fitting was confirmed by the chi-square evaluation (χ^2), which had values of the order of 10^{-3}.

Based on the electrical parameters, Ti-Zr alloys exhibited the highest polarization resistance and the lowest capacitance values ($p < 0.05$), indicating that a more resistant and protective oxide film was formed. The double etching proved to increase the materials' polarization resistance, especially for control groups, which means that this treatment provides the formation of a surface with better protection. In general, the chemical treatment generated slight changes in capacitance values. CpTi was the only material that presented a statistically significant improvement in this property after treatment ($p < 0.05$).

The potentiodynamic polarization results are in accordance with EIS measurements, since the Ti-Zr alloys presented a better passive behavior for the machined condition. This is evidenced by the shift of the polarization curves to more noble potentials (Fig. 11). All materials exhibited typical passive behavior of the curves. It can be observed from the curves that cpTi double etched surface reached a constant value of current density (passivation) faster and more easily than the other materials.

Based on the Tafel measurements, Ti-Zr alloys tend to exhibit more favorable values of the electrochemical parameters for machined surfaces (Table 5), such as reduced i_{corr} values ($p < 0.05$). Regarding the double etched surfaces, the chemical treatment was able to increase the E_{corr} to more electropositive values for all materials ($p < 0.05$); however, the etching process statistically improved only the i_{corr} parameter of cpTi. Concerning the i_{pass}, cpTi and Ti-10Zr alloy showed the smallest values.

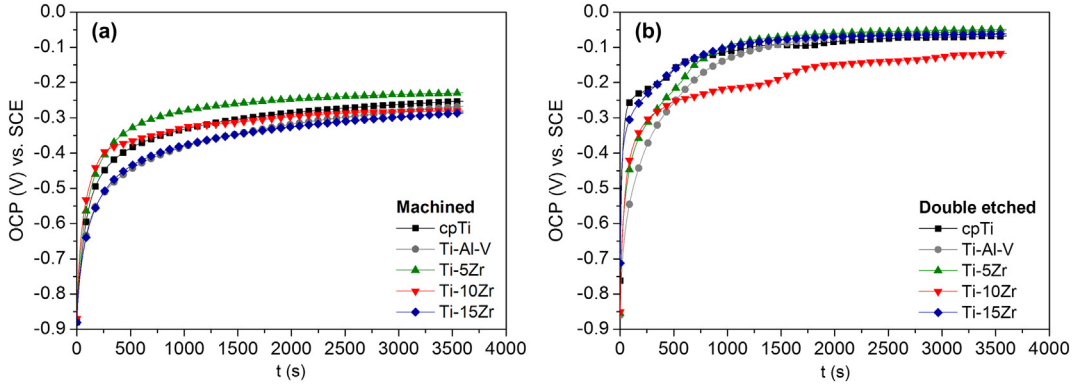

Fig. 8. OCPs of machined (a) and double etched (b) cpTi and Ti alloys surfaces as a function of time in SBF.

Table 3
Mean (and standard deviation) of open circuit potential of machined and double etched cpTi and Ti alloy surfaces (n = 5) after 1 h in SBF.

	Material	Open circuit potential
Machined	cpTi	−264.97 (13.68)^{bB}
	Ti-6Al-4V	−272.13 (17.88)^{bcB}
	Ti-5Zr	−230.80 (25.84)^{aB}
	Ti-10Zr	−273.94 (18.04)^{bcB}
	Ti-15Zr	−300.20 (14.81)^{cB}
Acid etched	cpTi	−67.72 (13.30)^{aA}
	Ti-6Al-4V	−67.06 (26.06)^{aA}
	Ti-5Zr	−61.87 (21.10)^{aA}
	Ti-10Zr	−131.40 (21.92)^{bA}
	Ti-15Zr	−70.46 (20.22)^{aA}

Means followed by different lowercase letters indicate statistically significant differences among the materials within each surface type. Means followed by different capital letters indicate statistically significant differences between the surfaces of each material ($p < 0.05$, Bonferroni test).

3.4. Cell morphology

Fig. 12 illustrates the most representative findings by SEM. After 96 h in culture, all the surfaces presented cells attached demonstrating that the used alloys were not detrimental to cell adhesion and proliferation, suggesting, therefore, that they are biocompatible. Qualitative analysis further suggested that surface condition (machined or acid etched) may affect cell morphology, with machined surface exhibiting stretched filopodia extensions and double etched surface showing a slightly more flattened and spread morphology. For Ti-10Zr and Ti-15Zr, the cells were oriented in the direction of the acicular structures. In addition, numerous filopodia extensions towards the holes of double etched surface suggested a strong cell attachment.

4. Discussion

Ti-Zr alloys have been developed to be used as alternative to cpTi and Ti-Al-V. In this study, we evaluated these materials with machined and etched surfaces. The experimental alloys presented greater electrochemical stability when compared to materials commercially used to manufacture dental implants. Additionally, the surface characteristics obtained by double acid etching, including complex topography, higher roughness, higher surface energy, and slight changes in cell morphology may indicate that intraosseous implants would have an enhanced in vivo biological response when implanted.

4.1. Surface characteristics and cell adhesion

Herein, the developed alloys presented the elemental concentrations very close to the stoichiometric values without presenting contaminants, which demonstrate their good quality [11,21,26]. Few differences were observed for the double etched surface as the increase of Zr content. This fact can be attributed to the higher resistance of this element to the acids used. In addition, previous study [27] showed that the etching process leads to selective enrichment of the β phase of Ti-Al-V alloy, leading to a V-rich surface. Possibly, in a similar way it can be occurred for Ti-Zr alloys and its α phase.

Regarding to the microstructure analyses, the Ti-Zr system exhibited an α microstructure that occurred as an equiaxed structure (Ti-5Zr) and as a typical Widmanstätten pattern (Ti-10Zr and Ti-15Zr) [11,21,28]. No indication of the existence of secondary phases was verified [21,28], since Zr acted as a neutral stabilizer. One of the main alterations found for the treated group is the identification of Ti hydride. This may have happened due to the reaction between metallic Ti atoms and free hydrogen ions in the acid solution [29,30]. When this structure is detected by XRD after acid etching, the hydrogen concentration in the surface should be considered to be very high [31] and does not necessarily

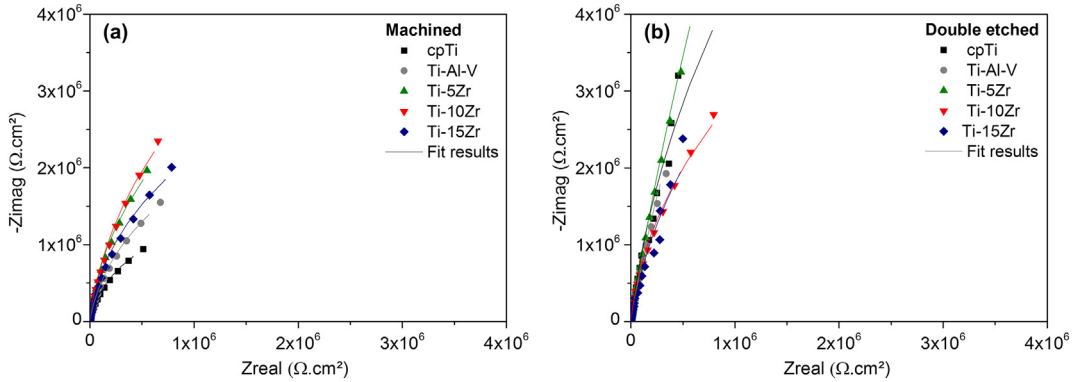

Fig. 9. Nyquist diagrams of machined (a) and double etched (b) cpTi and Ti alloy surfaces in SBF.

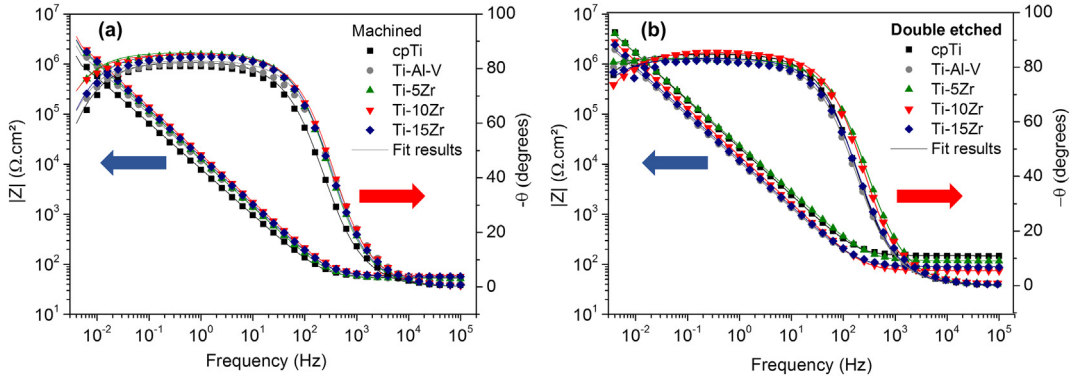

Fig. 10. Bode plots of machined (a) and double etched (b) cpTi and Ti alloy surfaces in SBF.

mean that the other materials did not present hydride formation. Besides, hydride was not observed by EDS because H atoms are too light to be detected by such a technique [29]. The presence of intermetallic compound and residual Zr for the other materials can also be related to the acid action on the surface.

In general, the microstructural features played a large role in how the acid etching altered the surface. Particularly, the grains size, orientation and shape were evidenced after double etching process for the Ti-Zr alloys. Previous studies [30,32] with SLA surfaces have shown that the substrate composition may influence the surface topography after treatment. Our results corroborate such findings regarding the behavior, as the nucleation of protrusions was more favorable on cpTi than on Ti-Zr system. It was already hypothesized that the hardness and grain size of the alloy can, in some way, influence the polishing process [21] and perhaps influence how the acid reacts with the surface as well. In addition to creating a complex microtopography, the chemical treatment increased the surface roughness and enhanced the effective interface areas of the materials [19,33,34]. This can provide long-term stability of the implant under loading [33] and may enhance the resistance to reverse torque removal due to the increased bone–implant contact and higher strength of osseointegration [18,35]. Among the groups, Ti-15Zr alloy double etched surface presented the highest average roughness. It is known that the acicular structures became coarser [28] and their amount increased as the Zr content increased [11], which may have influenced the roughness values due to the exposition of these structures after etching.

Another property that can be influenced by the nature of the bulk material is the surface energy. Ti-Zr alloys showed increased surface energy, which may affect protein adsorption, cell interactions, and the rate of osseointegration [36]. It has been reported previously [14] that subtle differences in the surface properties such as roughness, surface energy, and substrate composition were able to modulate the biological profile of Ti-50Zr alloy, which showed better response to the initial attachment of MC3T3-E1 osteoblast cells than cpTi. In our study, the association of a hydrophilic surface and topography with features at the micro- and submicron-scale, as seen for the double etched surface, was able to support cell adhesion. Interestingly, this type of surface modification has also been associated with increased cell proliferation and alkaline phosphatase expression [34], as well as with facilitated osteogenic cell retention and cell migration at the implant surface [35]. This is possibly because the first phase of cell–material interactions is regulated by the physicochemical surface properties [37].

4.2. Mechanical behavior

The mechanical properties of alloys are also sensitive to the alloy structure, depending fundamentally on the microstructure characteristics. Ti-Zr alloys were found to have statistically greater hardness. As previously reported [11,16,28,38], the increased hardness of Ti-Zr alloys is a consequence of solid-solution hardening generated by the α phase and also due to grain size refinement achieved by the thermomechanical process. A slight decrease in hardness with further increases in Zr content has been stated before [11,21,28] and also observed in our study. The etching process increased the hardness of almost all materials with exception of Ti-10Zr alloy. This result seems to be related to the appearance of residual Zr, since this alloy was the only one that did not present any new content on its microstructure.

Elastic modulus is an important property to implant materials and it should be comparable to that of bone tissue to prevent bone atrophy and to stimulate its remodeling by the effective load transfer and uniform stress distribution [39,40]. Most materials that have low elastic modulus are β Ti alloys [16]. At the same time, the material must to have adequate stiffness and resistance to support the forces to which implants are subjected without deforming. Herein, the α Ti-Zr alloys showed elastic modulus higher than that of cpTi, but similar values of stiffness. Meanwhile, they presented significantly lower values when

Table 4
Mean (and standard deviation) of electrical parameters obtained from the equivalent circuit models of machined and double etched cpTi and Ti alloy surfaces (n = 5).

Surface	Material	R_p (MΩ·cm²)	Q (S∗s^a cm^{-2}) × 10^{-5}	n	χ^2 × 10^{-3}
Machined	cpTi	4.08 (1.10)^{bB}	1.82 (0.18)^{aA}	0.93 (0.1)	1.37 (0.58)
	Ti-6Al-4V	4.58 (1.20)^{bB}	1.68 (0.27)^{aA}	0.92 (0.1)	2.29 (0.47)
	Ti-5Zr	11.10 (0.92)^{aB}	1.22 (0.10)^{bA}	0.94 (0.1)	1.43 (0.69)
	Ti-10Zr	12.32 (6.11)^{aA}	1.29 (0.16)^{bA}	0.94 (0.2)	0.95 (0.11)
	Ti-15Zr	9.81 (2.67)^{aB}	1.19 (0.15)^{bA}	0.94 (0.1)	1.61 (0.74)
Acid etched	cpTi	37.13 (8.30)^{aA}	0.93 (0.09)^{cB}	0.94 (0.1)	0.77 (0.46)
	Ti-6Al-4V	26.23 (24.51)^{abA}	1.62 (0.08)^{aA}	0.92 (0.1)	0.66 (0.13)
	Ti-5Zr	29.08 (8.57)^{abA}	1.33 (0.07)^{bA}	0.91 (0.1)	0.78 (0.60)
	Ti-10Zr	12.69 (5.21)^{cA}	1.17 (0.05)^{bcA}	0.93 (0.2)	0.60 (0.51)
	Ti-15Zr	18.24 (4.90)^{bcA}	1.29 (0.24)^{bA}	0.93 (0.1)	1.76 (0.92)

Means followed by different lowercase letters indicate statistically significant differences among the materials within each surface type. Means followed by different capital letters indicate statistically significant differences between the surfaces of each material type ($p < 0.05$, Bonferroni test).

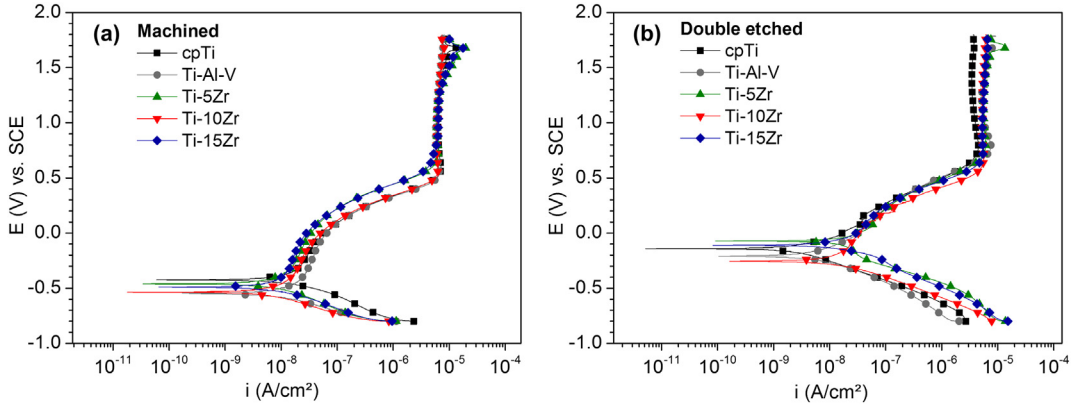

Fig. 11. Potentiodynamic polarization curves of machined (a) and double etched (b) cpTi and Ti alloy surfaces in SBF.

compared to Ti-Al-V. The heat treatment performed after swaging and consequently increase in hardness may be the main reason for the results found in the experimental alloys [21]. It is expected that materials with enhanced mechanical performance show better resistance to the degradation processes to which implants are subjected intra-orally, such as stresses during the implantation procedure (friction) as well as during their whole in vivo life (chewing load) [41]. Although hardness and elastic modulus are important properties of implant materials, other factors are also relevant for clinical application, such as wear resistance, fretting corrosion resistance, and mechanical/tensile strength [13], which should need to be further evaluated in future studies.

4.3. Electrochemical behavior

The understating of the corrosion kinetics of implant materials is extremely important as the intra-oral degradation processes can release metal ions to the environment, and in excess, these metal ions may be toxic or dangerous to the body [42]. The results obtained by the electrochemical tests indicate a positive influence of Zr addition on the material corrosion resistance, which may be related to a thicker and denser passive film on Ti-Zr alloys surfaces that are reinforced by ZrO_2 oxides [8,43]. Previous studies [21,28,44] have demonstrated the electrochemical superiority of alloys containing Zr. Besides reducing the anodic activity [45], Zr enhances the protection against oxidation [28]. Despite that, the higher hardness of these materials may have favored the maintenance of a thicker and more firmly adhered oxide layer on the surface [46].

The Ti-15Zr alloy presented notably lower capacitance, i_{corr} and i_{pass} values. This may be related to the fact that the presence of Zr oxides is proportional to the Zr concentration in the alloy [21], contributing to its improved electrochemical performance when compared to cpTi. This is in accordance with a previous study [28], where Ti-15Zr alloy had the fastest passivation tendency among Ti-Zr alloys. In general, such system has shown comparable or lower electrochemical activity and higher corrosion resistance than cpTi in different electrolytic solutions [8,12,28], as a consequence of improved protective properties of the passive film that acts as a barrier against the diffusion of ions [44,47]. Additionally, the amount of metal ions released decreased as the Zr proportion increased, indicating an oxide layer that is more stable and resistant to dissolution [12]. Although the electrochemical tests provide important parameters for the corrosive kinetics of materials, to establish the superiority of the experimental alloys it would be interesting to evaluate the interplay between corrosion and wear (i.e. tribocorrosion) of such system. The degradation process in the oral environment involves successive micro-movements in the implant/bone, implant/abutment and abutment/crown interfaces [48] that is better represented by the tribological contact simultaneously to corrosion.

With respect to the influence of the acid etching process on the materials electrochemical behavior, our previous study [49] has shown that etching with HCl and H_2O_2 seems to be an effective technique for enhancing the cpTi electrochemical stability. The HCl degrades the oxide film and reacts with the surface, forming a TiH intermediate layer, where a new oxide layer can be formed when in contact with moisture in the air [50]. It is believed that the combination of these two layers may be responsible for the improved potential, polarization resistance and E_{corr} values, which suggests improvement of the corrosion protection tendency and higher stability of the oxide layer in a corrosive environment when compared to the machined surface. Although statistically significant differences were not observed between the machined and double etched surface for the binary alloys, in some cases the capacitance and i_{corr} slightly increased. This behavior might be related to the increased surface roughness and surface area that is detrimental to the passive film formation, causing a higher

Table 5
Mean (and standard deviation) values of electrochemical parameters obtained from the potentiodynamic polarization curves of machined and double etched cpTi and Ti alloy surfaces (n = 5).

Surface	Group	E_{corr} (mV) vs. SCE	i_{corr} (nA cm^{-2})	b_a (V/decade)	$-b_c$ (V/decade)	i_{pass} (nA cm^{-2})
Machined	cpTi	−446.80 (25.79)^{aB}	16.11 (4.15)^{aA}	0.56 (0.03)	0.18 (0.01)	7.71 (0.71)^{aB}
	Ti-6Al-4V	−539.40 (57.49)^{cB}	15.82 (5.10)^{aA}	0.71 (0.03)	0.16 (0.02)	6.96 (0.95)^{abA}
	Ti-5Zr	−484.00 (23.37)^{abB}	7.94 (0.57)^{bA}	0.65 (0.05)	0.18 (0.02)	6.71 (0.28)^{bA}
	Ti-10Zr	−513.20 (26.86)^{bcB}	8.73 (2.47)^{bA}	0.68 (0.10)	0.16 (0.01)	7.15 (0.71)^{abB}
	Ti-15Zr	−509.20 (55.95)^{bcB}	7.32 (0.80)^{bA}	0.65 (0.13)	0.16 (0.02)	6.29 (0.73)^{bA}
Acid etched	cpTi	−172.33 (67.57)^{abcA}	6.44 (2.07)^{bB}	0.45 (0.15)	0.22 (0.02)	4.48 (0.39)^{cA}
	Ti-6Al-4V	−170.50 (18.82)^{bcA}	14.95 (3.14)^{aA}	0.46 (0.01)	0.30 (0.04)	7.03 (0.24)^{aA}
	Ti-5Zr	−115.43 (49.69)^{abA}	9.89 (1.58)^{bA}	0.29 (0.03)	0.20 (0.01)	5.90 (0.33)^{abA}
	Ti-10Zr	−212.60 (16.43)^{cA}	9.46 (1.37)^{bA}	0.36 (0.01)	0.18 (0.01)	5.72 (0.66)^{bA}
	Ti-15Zr	−110.13 (31.27)^{aA}	9.82 (1.07)^{bA}	0.38 (0.08)	0.21 (0.01)	6.31 (1.09)^{abA}

Means followed by different lowercase letters indicate statistically significant differences among the materials within each surface type. Means followed by different capital letters indicate statistically significant differences between the surfaces of each material type ($p < 0.05$, Bonferroni test).

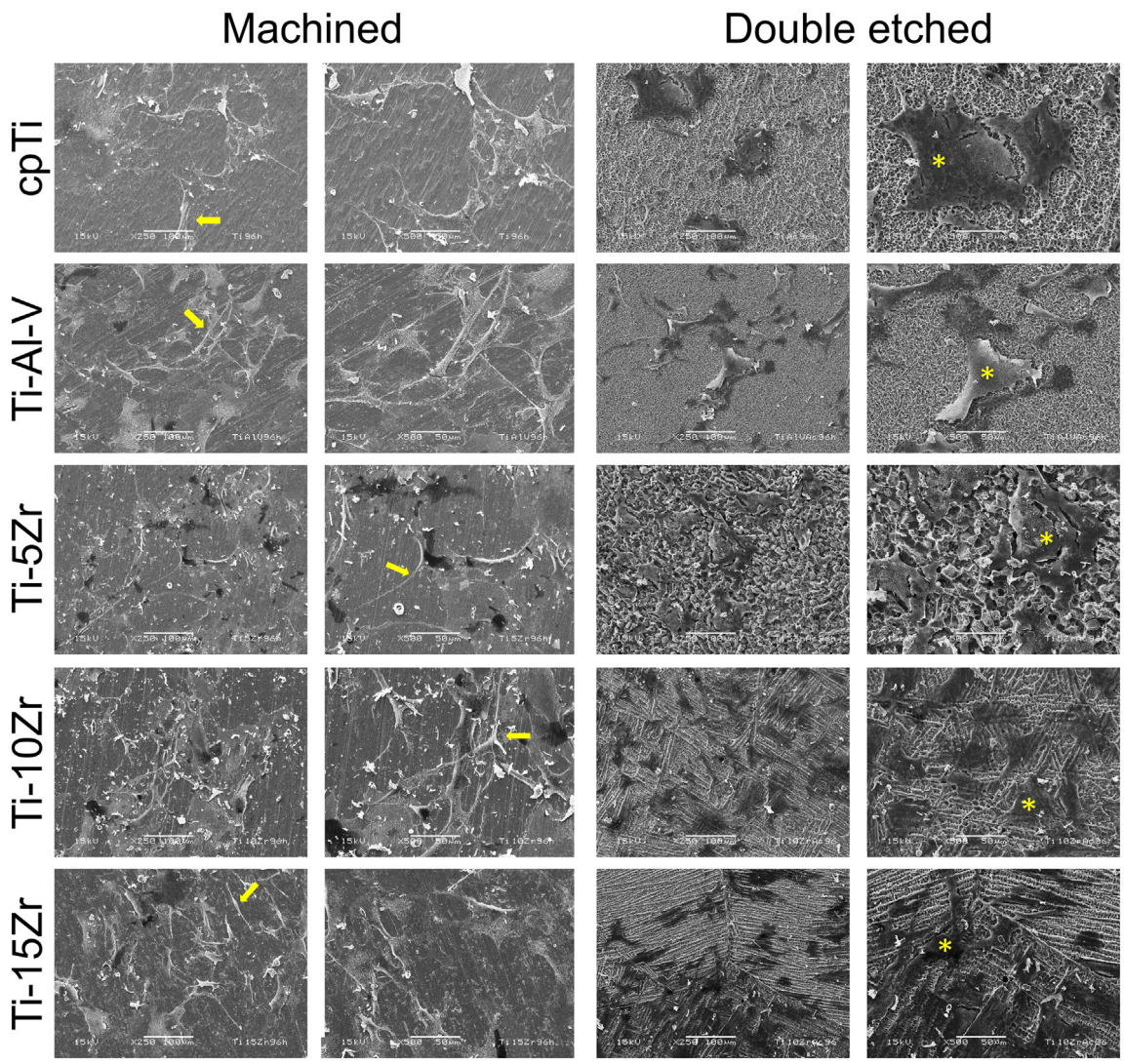

Fig. 12. Micrographs of MC3T3 cultured on machined and double etched cpTi and Ti alloy surfaces for 96 h. Arrows indicate elongated cells, whereas asterisks show spread-shaped ones.

susceptibility to pitting corrosion [51]. Also, it is known that an improved wettability can result in lower contact resistance between the electrode and electrolyte [52], which may have contributed towards the current density increase of treated surfaces. Despite this, there was not a clear correlation between the observed differences of corrosion parameters with the contact angle values as all surfaces exhibited a hydrophilic behavior. Controlling the surface wettability making it more hydrophobic has proved to be an important strategy to inhibit corrosion in metals [53]. It is an important area to be explored in the biomedical implants with the aim to control the ionic exchanges between the metal-based implant and the environment. However, hydrophobic surface may mitigate cell adhesion and spreading. Therefore, it is necessary to balance the wettability of dental implants to reduce its chemical degradation but at the same time to not affect its biocompatibility.

5. Conclusions

Binary Ti-Zr alloys with different concentrations of Zr (5, 10, and 15 wt%) were studied as a function of two features of the surfaces (machined and double etched). The addition of Zr to Ti improved the mechanical and surface properties when compared to cpTi and Ti-Al-V alloy. The experimental alloys showed better electrochemical behavior due to decreases in the capacitance, i_{corr} and i_{pass}, and implemented slight changes in cell morphology. The double acid etching treatment was beneficial for the mechanical behavior, surface properties, cell adhesion and proliferation, as well as for the corrosion potential and polarization resistance parameters.

Acknowledgments

This work was supported by the Sao Paulo Research Foundation (FAPESP), Brazil (grant numbers 2013/15545-2, 2013/08451-1, 2014/23575-1, 2015/25562-7, 2015/03159-6, and 2016/11470-6) and The Brazilian National Council for Scientific and Technological Development (CNPq), Brazil (grant number 311203/2013-2). The authors would also like to express their gratitude to Dr Mathew T Mathew from the Department of Biomedical Sciences College of Medicine at Rockford, University of Illinois for the donation of the electrochemical cell, Rafael Parra and Jéssica Gonçalves for their contribution and support at the Laboratory of Technological Plasmas at Universidade Estadual Paulista (UNESP) and to Elton José de Souza from the Department of Physics and Chemistry at UNESP for the AFM facility.

References

[1] M. Geetha, A.K. Singh, R. Asokamani, A.K. Gogia, Ti based biomaterials, the ultimate choice for orthopaedic implants – a review, Prog. Mater. Sci. 54 (2009) 397–425, https://doi.org/10.1016/j.pmatsci.2008.06.004.

[2] H.M. Grandin, S. Berner, M. Dard, A review of titanium zirconium (TiZr) alloys for use in endosseous dental implants, Materials (Basel) 5 (2012) 1348–1360, https://doi.org/10.3390/ma5081348.

[3] P. Stenlund, O. Omar, U. Brohede, S. Norgren, B. Norlindh, A. Johansson, J. Lausmaa, P. Thomsen, A. Palmquist, Bone response to a novel Ti–Ta–Nb–Zr alloy, Acta Biomater. 20 (2015) 165–175, https://doi.org/10.1016/j.actbio.2015.03.038.

[4] K. Shemtov-Yona, D. Rittel, On the mechanical integrity of retrieved dental implants, J. Mech. Behav. Biomed. Mater. 49 (2015) 290–299, https://doi.org/10.1016/j.jmbbm.2015.05.014.

[5] K. Shemtov-yona, D. Rittel, Identification of failure mechanisms in retrieved fractured dental implants, Eng. Fail. Anal. 38 (2014) 58–65, https://doi.org/10.1016/j.engfailanal.2014.01.002.

[6] S.X. Liang, X.J. Feng, L.X. Yin, X.Y. Liu, M.Z. Ma, R.P. Liu, Development of a new β Ti alloy with low modulus and favorable plasticity for implant material, Mater. Sci. Eng. C 61 (2016) 338–343, https://doi.org/10.1016/j.msec.2015.12.076.

[7] Y. Manor, S. Oubaid, O. Mardinger, G. Chaushu, J. Nissan, Characteristics of early versus late implant failure: a retrospective study, J. Oral Maxillofac. Surg. 67 (2009) 2649–2652, https://doi.org/10.1016/j.joms.2009.07.050.

[8] J.M. Calderon-Moreno, C. Vasilescu, S.I. Drob, S. Ivanescu, P. Osiceanu, P. Drob, M. Popa, S. Preda, E. Vasilescu, Microstructural and mechanical properties, surface and electrochemical characterisation of a new Ti–Zr–Nb alloy for implant applications, J. Alloys Compd. 612 (2014) 398–410, https://doi.org/10.1016/j.jallcom.2014.05.159.

[9] A.M. Kaufman, C.I. Alabre, H.E. Rubash, A.S. Shanbhag, Human macrophage response to UHMWPE, TiAlV, CoCr, and alumina particles: analysis of multiple cytokines using protein arrays, J. Biomed. Mater. Res. Part A 84A (2008) 464–474, https://doi.org/10.1002/jbm.a.31467.

[10] M. Noronha Oliveira, W.V.H. Schunemann, M.T. Mathew, B. Henriques, R.S. Magini, W. Teughels, J.C.M. Souza, Can degradation products released from dental implants affect peri-implant tissues? J. Periodontal Res. 53 (2018) 1–11, https://doi.org/10.1111/jre.12479.

[11] D.R.N. Correa, F.B. Vicente, T.A.G. Donato, V.E. Arana-Chavez, M.A.R. Buzalaf, C.R. Grandini, The effect of the solute on the structure, selected mechanical properties, and biocompatibility of Ti-Zr system alloys for dental applications, Mater. Sci. Eng. C 34 (2014) 354–359, https://doi.org/10.1016/j.msec.2013.09.032.

[12] T. Akimoto, T. Ueno, Y. Tsutsumi, H. Doi, T. Hanawa, N. Wakabayashi, Evaluation of corrosion resistance of implant-use Ti-Zr binary alloys with a range of compositions, J. Biomed. Mater. Res. B Appl. Biomater. 106 (2018) 73–79, https://doi.org/10.1002/jbm.b.33811.

[13] Y. Ikarashi, K. Toyoda, E. Kobayashi, H. Doi, T. Yoneyama, H. Hamanaka, T. Tsuchiya, Improved biocompatibility of titanium-zirconium (Ti-Zr) alloy: tissue reaction and sensitization to Ti-Zr alloy compared with pure Ti and Zr in rat implantation study, J. Japan Inst. Met. 71 (2007) 395–401, https://doi.org/10.2320/jinstmet.71.395.

[14] S. Sista, C. Wen, P.D. Hodgson, G. Pande, The influence of surface energy of titanium-zirconium alloy on osteoblast cell functions in vitro, J. Biomed. Mater. Res. A 97 (2011) 27–36, https://doi.org/10.1002/jbm.a.33013.

[15] S. Barter, P. Stone, U. Brägger, A pilot study to evaluate the success and survival rate of titanium-zirconium implants in partially edentulous patients: results after 24 months of follow-up, Clin. Oral Implants Res. 23 (2012) 873–881, https://doi.org/10.1111/j.1600-0501.2011.02231.x.

[16] J.M. Cordeiro, V.A.R. Barão, Is there scientific evidence favoring the substitution of commercially pure titanium with titanium alloys for the manufacture of dental implants? Mater. Sci. Eng. C 71 (2017) 1201–1215, https://doi.org/10.1016/j.msec.2016.10.025.

[17] X. Shi, L. Xu, K.B. Violin, S. Lu, Improved osseointegration of long-term stored SLA implant by hydrothermal sterilization, J. Mech. Behav. Biomed. Mater. 53 (2016) 312–319, https://doi.org/10.1016/j.jmbbm.2015.08.038.

[18] S. Cho, The removal torque of titanium screw inserted in rabbit tibia treated by dual acid etching, Biomaterials 24 (2003) 3611–3617, https://doi.org/10.1016/S0142-9612(03)00218-7.

[19] D.P. Oliveira, A. Palmieri, F. Carinci, C. Bolfarini, Gene expression of human osteoblasts cells on chemically treated surfaces of Ti–6Al–4V–ELI, Mater. Sci. Eng. C 51 (2015) 248–255, https://doi.org/10.1016/j.msec.2015.03.011.

[20] L.P. Faverani, W.G. Assunção, P.S.P. de Carvalho, J.C.-C. Yuan, C. Sukotjo, M.T. Mathew, V.A. Barao, Effects of dextrose and lipopolysaccharide on the corrosion behavior of a Ti-6Al-4V alloy with a smooth surface or treated with double-acid-etching, PLoS One 9 (2014) e93377, , https://doi.org/10.1371/journal.pone.0093377.

[21] J.M. Cordeiro, T. Beline, A.L.R. Ribeiro, E.C. Rangel, N.C. da Cruz, R. Landers, L.P. Faverani, L.G. Vaz, L.M.G. Fais, F.B. Vicente, C.R. Grandini, M.T. Mathew, C. Sukotjo, V.A.R. Barão, Development of binary and ternary titanium alloys for dental implants, Dent. Mater. 33 (2017) 1244–1257, https://doi.org/10.1016/j.dental.2017.07.013.

[22] J.M. Cordeiro, H.N. Pantaroto, E.M. Paschoaleto, E.C. Rangel, N.C. da Cruz, C. Sukotjo, V.A.R. Barão, Synthesis of biofunctional coating for a TiZr alloy: surface, electrochemical, and biological characterizations, Appl. Surf. Sci. 452 (2018) 268–278, https://doi.org/10.1016/j.apsusc.2018.05.044.

[23] V.A.R. Barão, M.T. Mathew, W.G. Assunção, J.C.-C. Yuan, M.A. Wimmer, C. Sukotjo, Stability of cp-Ti and Ti-6Al-4V alloy for dental implants as a function of saliva pH - an electrochemical study, Clin. Oral Implants Res. 23 (2012) 1055–1062, https://doi.org/10.1111/j.1600-0501.2011.02265.x.

[24] L. Muller, F.A. Muller, Preparation of SBF with different HCO_3^- content and its influence on the composition of biomimetic apatites, Acta Biomater. 2 (2006) 181–189, https://doi.org/10.1016/j.actbio.2005.11.001.

[25] A.O. Matos, A.P. Ricomini-Filho, T. Beline, E.S. Ogawa, B.E. Costa-Oliveira, A.B. de Almeida, F.H. Nociti Junior, E.C. Rangel, N.C. da Cruz, C. Sukotjo, M.T. Mathew, V.A.R. Barão, Three-species biofilm model onto plasma-treated titanium implant surface, Colloids Surf. B: Biointerfaces 152 (2017) 354–366, https://doi.org/10.1016/j.colsurfb.2017.01.035.

[26] P.A.B. Kuroda, M.A.R. Buzalaf, C.R. Grandini, Effect of molybdenum on structure, microstructure and mechanical properties of biomedical Ti-20Zr-Mo alloys, Mater. Sci. Eng. C 67 (2016) 511–515, https://doi.org/10.1016/j.msec.2016.05.053.

[27] N. Saulacic, D.D. Bosshardt, M.M. Bornstein, S. Berner, D. Buser, Bone apposition to a titanium-zirconium alloy implant, as compared to two other titanium-containing implants, Eur. Cell. Mater. 23 (2012) 273–278.

[28] M.-K. Han, M. Hwang, M. Yang, H. Yang, H.-J. Song, Y.-J. Park, Effect of zirconium content on the microstructure, physical properties and corrosion behavior of Ti alloys, Mater. Sci. Eng. A 616 (2014) 268–274, https://doi.org/10.1016/j.msea.2014.08.010.

[29] N. Ren, G. Wang, H. Liu, T. Ohachi, In situ synthesis of TiH2 layer on metallic titanium foil through gaseous hydrogen free acid-hydrothermal method, Mater. Res. Bull. 50 (2014) 379–384, https://doi.org/10.1016/j.materresbull.2013.11.002.

[30] M. Murphy, M.S. Walczak, A.G. Thomas, N. Silikas, S. Berner, R. Lindsay, M. Murphy, M.S. Walczak, A.G. Thomas, N. Silikas, S. Berner, R. Lindsay, Toward optimizing dental implant performance: surface characterization of Ti and TiZr implant materials, Dent. Mater. 33 (2016) 43–53, https://doi.org/10.1016/j.dental.2016.10.001.

[31] A. Nagaoka, K. Yokoyama, J. Sakai, Evaluation of hydrogen absorption behaviour during acid etching for surface modification of commercial pure Ti, Ti–6Al–4V and Ni–Ti superelastic alloys, Corros. Sci. 52 (2010) 1130–1138, https://doi.org/10.1016/j.corsci.2009.12.029.

[32] M.J. Frank, M.S. Walter, S.P. Lyngstadaas, E. Wintermantel, H.J. Haugen, Hydrogen content in titanium and a titanium–zirconium alloy after acid etching, Mater. Sci. Eng. C 33 (2013) 1282–1288, https://doi.org/10.1016/j.msec.2012.12.027.

[33] J.E. Davies, E. Ajami, R. Moineddin, V.C. Mendes, The roles of different scale ranges of surface implant topography on the stability of the bone/implant interface, Biomaterials 34 (2013) 3535–3546, https://doi.org/10.1016/j.biomaterials.2013.01.024.

[34] L. Giner, M. Mercadé, S. Torrent, M. Punset, R.A. Pérez, L.M. Delgado, F.J. Gil, Double acid etching treatment of dental implants for enhanced biological properties, J. Appl. Biomater. Funct. Mater. 16 (2018) 83–89, https://doi.org/10.5301/jabfm.5000376.

[35] C.N. Elias, Y. Oshida, J.H.C. Lima, C.A. Muller, Relationship between surface properties (roughness, wettability and morphology) of titanium and dental implant removal torque, J. Mech. Behav. Biomed. Mater. 1 (2008) 234–242, https://doi.org/10.1016/j.jmbbm.2007.12.002.

[36] R.A. Gittens, L. Scheideler, F. Rupp, S.L. Hyzy, J. Geis-Gerstorfer, Z. Schwartz, B.D. Boyan, A review on the wettability of dental implant surfaces II: biological and clinical aspects, Acta Biomater. 10 (2014) 2907–2918, https://doi.org/10.1016/j.actbio.2014.03.032.

[37] S. Sista, A. Nouri, Y. Li, C. Wen, P.D. Hodgson, G. Pande, Cell biological responses of osteoblasts on anodized nanotubular surface of a titanium-zirconium alloy, J. Biomed. Mater. Res. Part A 101 (2013) 3416–3430, https://doi.org/10.1002/jbm.a.34638.

[38] A.E. Medvedev, A. Molotnikov, R. Lapovok, R. Zeller, S. Berner, P. Habersetzer, F. Dalla Torre, F. Dalla, Microstructure and mechanical properties of Ti–15Zr alloy used as dental implant material, J. Mech. Behav. Biomed. Mater. 62 (2016) 384–398, https://doi.org/10.1016/j.jmbbm.2016.05.008.

[39] M. Niinomi, M. Nakai, J. Hieda, Development of new metallic alloys for biomedical applications, Acta Biomater. 8 (2012) 3888–3903, https://doi.org/10.1016/j.actbio.2012.06.037.

[40] K.C. Nune, R.D.K. Misra, S.J. Li, Y.L. Hao, R. Yang, Osteoblast cellular activity on low elastic modulus Ti–24Nb–4Zr–8Sn alloy, 3 (2016) 152–165, https://doi.org/10.1016/j.dental.2016.11.005.

[41] S. Ferraris, A. Bobbio, M. Miola, S. Spriano, Micro- and nano-textured, hydrophilic and bioactive titanium dental implants, Surf. Coat. Technol. 276 (2015) 374–383, https://doi.org/10.1016/j.surfcoat.2015.06.042.

[42] R.I.M.M. Asri, W.S.W.W. Harun, M. Samykano, N.A.C.C. Lah, S.A.C.C. Ghani, F. Tarlochan, M.R. Raza, Corrosion and surface modification on biocompatible metals: a review, Mater. Sci. Eng. C 77 (2017) 1261–1274, https://doi.org/10.1016/j.msec.2017.04.102.

[43] E.A. Ferreira, R.C. Rocha-Filho, S.R. Biaggio, N. Bocchi, Corrosion resistance of the Ti–50Zr at.% alloy after anodization in different acidic electrolytes, Corros. Sci. 52 (2010) 4058–4063, https://doi.org/10.1016/j.corsci.2010.08.021.

[44] J.M. Calderon Moreno, E. Vasilescu, P. Drob, P. Osiceanu, C. Vasilescu, S.I. Drob, M. Popa, Surface analysis and electrochemical behavior of Ti–20Zr alloy in simulated physiological fluids, Mater. Sci. Eng. B 178 (2013) 1195–1204, https://doi.org/10.1016/j.mseb.2013.07.006.

[45] Z.B. Wang, H.X. Hu, Y.G. Zheng, W. Ke, Y.X. Qiao, Comparison of the corrosion behavior of pure titanium and its alloys in fluoride-containing sulfuric acid, Corros. Sci. 103 (2016) 50–65, https://doi.org/10.1016/j.corsci.2015.11.003.

[46] I. Cvijović-Alagić, Z. Cvijović, S. Mitrović, V. Panić, M. Rakin, Wear and corrosion behaviour of Ti–13Nb–13Zr and Ti–6Al–4V alloys in simulated physiological solution, Corros. Sci. 53 (2011) 796–808, https://doi.org/10.1016/j.corsci.2010.11.014.

[47] J.M. Calderon Moreno, P. Osiceanu, C. Vasilescu, M. Anastasescu, S.I. Drob, M. Popa, Obtaining, structural and corrosion characterization of anodized nanolayers on Ti-20Zr alloy surface, Surf. Coat. Technol. 235 (2013) 792–802, https://doi.org/10.1016/j.surfcoat.2013.09.006.

[48] Z. Wang, Y. Zhou, H. Wang, Y. Li, W. Huang, Tribocorrosion behavior of Ti-30Zr alloy for dental implants, Mater. Lett. 218 (2018) 190–192, https://doi.org/10.1016/j.matlet.2018.02.008.

[49] E.S. Ogawa, A.O. Matos, T. Beline, I.S.V. Marques, C. Sukotjo, M.T. Mathew, E.C. Rangel, N.C. Cruz, M.F. Mesquita, R.X. Consani, V.A.R. Barão, Surface-treated commercially pure titanium for biomedical applications: electrochemical, structural, mechanical and chemical characterizations, Mater. Sci. Eng. C 65 (2016) 251–261, https://doi.org/10.1016/j.msec.2016.04.036.

[50] L. Jonášová, F.A. Müller, A. Helebrant, J. Strnad, P. Greil, Biomimetic apatite formation on chemically treated titanium, Biomaterials 25 (2004) 1187–1194, https://doi.org/10.1016/j.biomaterials.2003.08.009.

[51] V. Barranco, M.L. Escudero, M.C. García-Alonso, 3D, chemical and electrochemical characterization of blasted TI6Al4V surfaces: its influence on the corrosion behaviour, Electrochim. Acta 52 (2007) 4374–4384, https://doi.org/10.1016/j.electacta.2006.12.031.

[52] Q. Abbas, M. Mirzaeian, A.A. Ogwu, M. Mazur, D. Gibson, Effect of physical activation/surface functional groups on wettability and electrochemical performance of carbon/activated carbon aerogels based electrode materials for electrochemical capacitors, Int. J. Hydrog. Energy (2018) 1–10, https://doi.org/10.1016/j.ijhydene.2018.04.099.

[53] E. Vazirinasab, R. Jafari, G. Momen, Application of superhydrophobic coatings as a corrosion barrier: a review, Surf. Coat. Technol. 341 (2018) 40–56, https://doi.org/10.1016/j.surfcoat.2017.11.053.